Journal of Medicinal Chemistry

pubs.acs.org/jmc Article

Discovery of the Next-Generation Pan-TRK Kinase Inhibitors for the Treatment of Cancer

Zongliang Liu, Pengfei Yu, Lin Dong, Wenyan Wang, Sijin Duan, Bingsi Wang, Xiaoyan Gong, Liang Ye, Hongbo Wang,* and Jingwei Tian*

Cite This: *J. Med. Chem.* 2021, 64, 10286−10296 Read Online

ACCESS | Metrics & More | Article Recommendations | Supporting Information

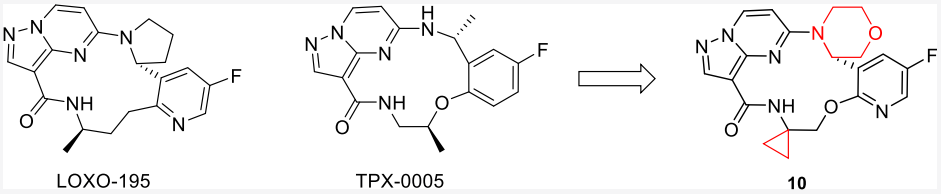

ABSTRACT: The neurotrophic receptor tyrosine kinase (NTRK) genes including NTRK1, NTRK2, and NTRK3 encode the tropomyosin receptor kinase (Trk) proteins TrkA, TrkB, and TrkC, respectively. So far, two TRK inhibitors, larotrectinib sulfate (LOXO-101 sulfate) and entrectinib (NMS-E628, RXDX-101), have been approved for clinical use in 2018 and 2019, respectively. To overcome acquired resistance, next-generation Trk inhibitors such as selitrectinib (LOXO-195) and repotrectinib (TPX-0005) have been developed and exhibit effectiveness to induce remission in patients with larotrectinib treatment failure. Herein, we report the identification and optimization of a series of macrocyclic compounds as potent pan-Trk (WT and MT) inhibitors that exhibited excellent physiochemical properties and good oral pharmacokinetics. Compound **10** was identified *via* optimization from the aspects of chemistry and pharmacokinetic properties, which showed good activity against wild and mutant TrkA/TrkC in *in vitro* and *in vivo* studies.

Downloaded via CALIFORNIA INST OF TECHNOLOGY on August 11, 2021 at 16:07:46 (UTC).
See https://pubs.acs.org/sharingguidelines for options on how to legitimately share published articles.

INTRODUCTION

In order to improve the efficacy of anti-tumor drugs and reduce their side effects, cancer treatment is shifting toward precision oncology. As such, patients receive individualized therapy based on the prescreening of predictive biomarkers, such as oncogenic mutations, rather than using empiric chemotherapy. It was reported in 2007 that gene fusions account for 20% of human cancer morbidity.[1] The neurotrophic receptor tyrosine kinase (NTRK) genes including NTRK1, NTRK2, and NTRK3 encode the tropomyosin receptor kinase (Trk) proteins TrkA, TrkB, and TrkC, respectively.[2] NTRK rearrangements and fusion gene products have been observed in numerous tumor types.[3] For example, NTRK fusions are found in about 50% of pediatric diffuse intrinsic pontine glioma and non-brainstem glioblastoma,[4] 16.7% of thyroid carcinoma,[5] 7.1% of pediatric gliomas,[6] 3.3% of lung cancers,[7] 2.5% of glioblastomas, and 2.2% of colorectal cancer.[6,8]

The growing number of identified gene fusions involving the NTRK gene drew the interest of the scientific community to develop gene-specific anti-cancer drugs. So far, two TRK inhibitors, larotrectinib sulfate (LOXO-101 sulfate) and entrectinib (NMS-E628, RXDX-101), have been approved for clinical use in 2018 and 2019, respectively, and many are currently under clinical trials (Figure 1). Entrectinib is a potent, orally available, and central nervous system-active pan-

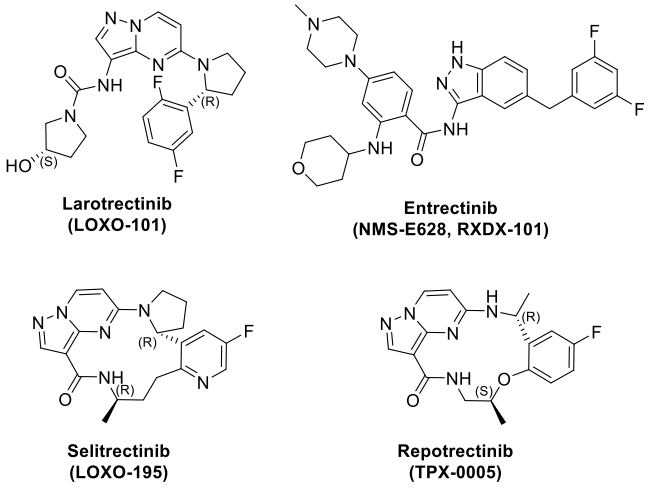

Figure 1. Trk inhibitors approved and in clinical trials.

Received: April 19, 2021
Published: July 13, 2021

ACS Publications © 2021 American Chemical Society

Trk, ROS1, and ALK inhibitor. Entrectinib inhibits TrkA, TrkB, TrkC, ROS1, and ALK with IC_{50} values of 1, 3, 5, 12, and 7 nM, respectively.[9] Larotrectinib is an adenosine triphosphate (ATP)-competitive orally active pan-Trk inhibitor, with IC_{50} values of 2−20 nmol/L against cancer cells and between 5 and 11 nM against all three isoforms, and with 1000-fold or greater selectivity relative to other kinases.[10] The first 55 patients with solid tumors with the confirmed NTRK gene fusion were enrolled in one of the three multicenter, open-label, single-arm clinical trials (NCT02122913, NCT02637687, and NCT02576431). Of all the enrolled patients with confirmatory response data available, the objective response rate was 76, with 12% complete response and 64% partial response (information from the drug label).

One major limitation to maintain durable therapeutic efficacy for all kinase inhibitors is the acquired resistance. To overcome acquired resistance, next-generation Trk inhibitors such as selitrectinib (LOXO-195) and repotrectinib (TPX-0005) have been developed, which exhibited effectiveness to induce remission in patients with larotrectinib treatment failure (Figure 1).[11,12] LOXO-195 shows strong binding to the wild-type TrkA, TrkB, and TrkC kinase domains and has potent (IC_{50} < 1 nM) inhibitory activity in kinase enzyme assays.[11] Importantly, LOXO-195 achieves low nanomolar inhibitory activity against $TrkA^{G595R}$, $TrkA^{G667C}$, $TrkC^{G623R}$, and $TrkC^{G696A}$, with IC_{50} values being 2.0, 9.8, 2.3, and 2.5 nM, respectively, but showed little effect on 228 other different kinases. In an *in vitro* efficacy study, LOXO-195 demonstrated potent inhibition of cell proliferation in Trk fusion-containing KM12, CUTO-3, and MO-91 cell lines ($IC_{50} \leq 5$ nM).[11] TPX-0005 is a multi-kinase inhibitor which shows potent effects against ROS1 (IC_{50} = 0.07 nM), Trk (IC_{50} = 0.83/0.05/0.1 nM for TrkA/B/C), WT ALK (IC_{50} = 1.01 nM), and JAK2 (IC_{50} = 1.04 nM).[12] Both LOXO-195 and TPX-0005 demonstrated significant efficacy in clinical trials in patients who were resistant to the first-generation Trk inhibitors.[11−14]

In this study, we report the identification and optimization of a series of macrocyclic compounds as potent pan-Trk (WT and MT) inhibitors that exhibited excellent physiochemical properties and good oral pharmacokinetics.

RESULTS AND DISCUSSION

Docking of LOXO-195 and TPX-0005 with TrkA. Currently, the cocrystal structures of LOXO-101 or LOXO-195 with Trk protein remain unknown. We docked LOXO-195 and TPX-0005 to explore their binding conformation with the TrkA protein by using Discovery Studio 2018 software (CDOCKER) and the existing eutectic complex (PDB ID: 4YNE).[15] From the docking test, we found that the binding modes of LOXO-195 and TPX-0005 with TrkC are nearly identical (Figure 2). The nitrogen atom on the pyrazole ring can form a hydrogen bond with Met592 in the hinge area. The fluorophenyl/fluoropyridine moiety that was well integrated into the hydrophobic pocket maintained a vertical conformation with the entire skeleton and had hydrophobic interactions with the surrounding Phe521, Leu657, Gly667, and Asp668. Simultaneously, the fluorine atom formed a key interaction force with Asn655. The oxygen atom on the amide formed a hydrogen bond with Met592 in the hinge region through the water molecule. There was a hydrophobic effect between the tetrahydropyrrole of LOXO-195 with the gatekeepers Phe589 and Phe521. The methyl group at the same position of TPX-0005 also had a hydrophobic effect with Phe521. The same

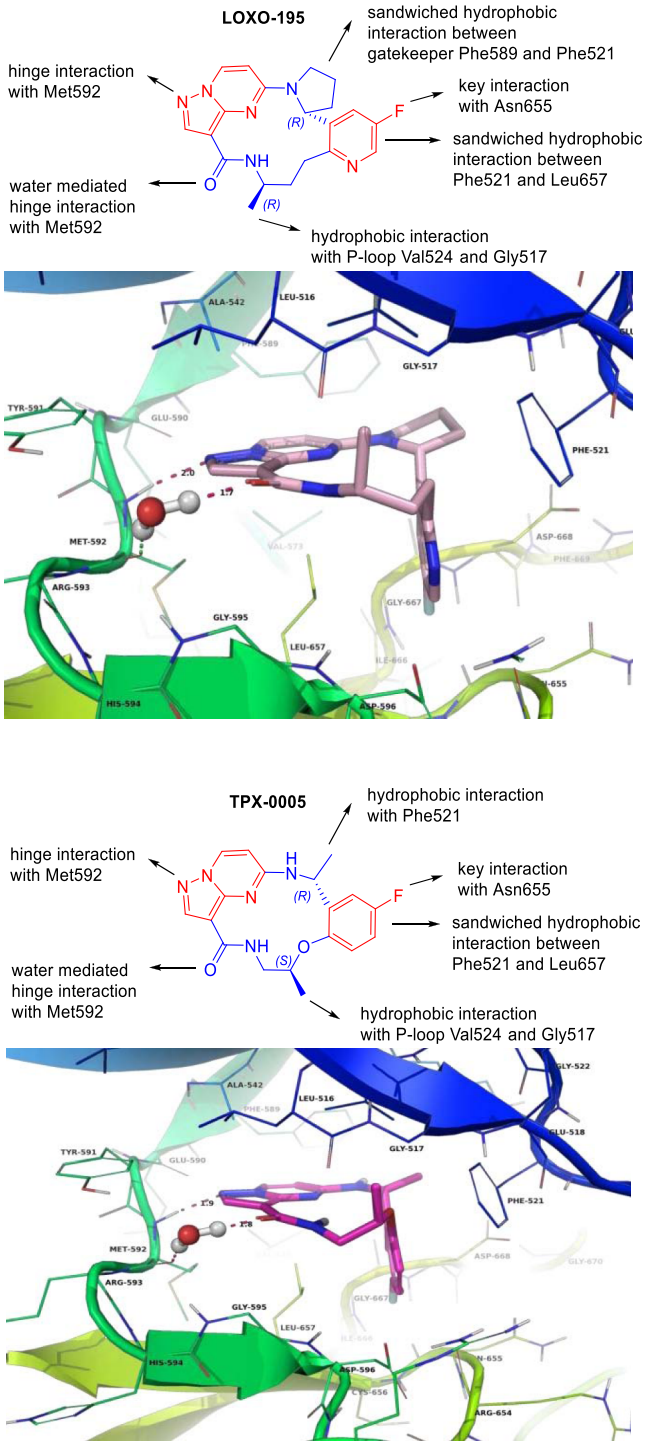

Figure 2. Docking of LOXO-195 and TPX-0005 with TrkA.

hydrophobic interaction existed between the remaining methyl groups of LOXO-195 and TPX-0005 with P-loop Val524 and Gly517. The structures of the hinge region and the fluoropyridine/fluorobenzene region (marked in red) were relatively conservative, which plays a decisive role in the activity of Trk kinase. The tetrahydropyrrole region and the amide alkyl chain (marked in blue) were more flexible and there was chemical space for structural modification. Therefore, we mainly modified the blue area of the structure in order to obtain preclinical drug candidates with better activity and selectivity.

https://doi.org/10.1021/acs.jmedchem.1c00712
J. Med. Chem. 2021, 64, 10286−10296

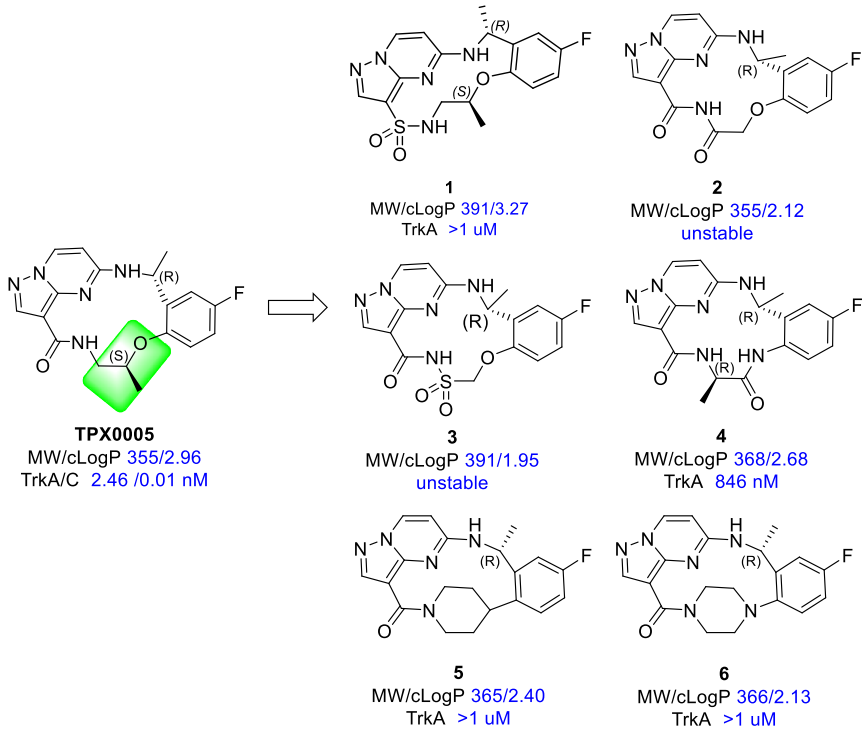

Figure 3. Structure−activity relationship of TPX-0005.

Table 1. PD Data of Compounds 8, 9, and 10 *In Vitro*

		compound (IC_{50} nM)				
		LOXO-195	TPX-0005	**8**	**9**	**10**
enzymatic	TrkA	6.7 ± 0.5	2.5 ± 0.4	3.2 ± 0.6	4.9 ± 0.4	2.4 ± 0.3
	$TrkA^{G595R}$	6.2 ± 0.5	1.4 ± 0.2	2.1 ± 0.4	9.4 ± 1.0	3.5 ± 0.5
	$TrkA^{G667C}$	110.0 ± 10.1	8.7 ± 0.8	0.7 ± 0.1	1.7 ± 0.3	2.3 ± 0.3
	TrkC	0.5 ± 0.1	0.01 ± 0.00	0.2 ± 0.0	0.2 ± 0.1	0.2 ± 0.1
	ALK	274.0 ± 16.4	2.3 ± 0.4	18.5 ± 0.7	88.9 ± 12.5	182.0 ± 14.2
	Ros1	1.15 ± 0.07	0.17 ± 0.05	0.2 ± 0.1	1.2 ± 0.3	1.0 ± 0.3
cellular	Ba/F3 TrkA	4.9 ± 0.3	1.8 ± 0.3	0.2 ± 0.0	0.6 ± 0.1	0.6 ± 0.1
	Ba/F3 $TrkA^{G595R}$	6.8 ± 0.7	8.0 ± 0.6	0.4 ± 0.0		7.7 ± 0.5
	Ba/F3 $TrkA^{F589L}$	25.4 ± 4.5	0.7 ± 0.2			4.9 ± 0.2
	Ba/F3 $TrkA^{G667A}$	24.4 ± 2.5				0.8 ± 0.1
	Ba/F3 $TrkC^{G623R}$	2.7 ± 0.5	4.8 ± 0.4	5.8 ± 0.3		2.7 ± 0.2
	Ba/F3 SLC34A2-Ros1	36.7 ± 3.6	2.2 ± 0.4	12.6 ± 0.7		2.3 ± 0.3

Structure−Activity Relationship of TPX-0005. We first studied the structure−activity relationship of TPX-0005. The amide group in TPX-0005 was replaced with a sulfonamide group (compound **1**, Figure 3), which led to the loss of its activity. Maintaining the chain length between the amide and fluorophenyl groups, the structure modification was carried out to obtain compounds **2**, **3**, **4**, **5**, and **6** (Figure 3). Compounds **2** and **3** with imide and sulfonimide were unstable likely due to the increased ring tension. Changing the ether bond to an amide group (compound **4**) reduced the TrkA inhibitory activity by 300−400 times. When piperazine or piperidine was used for bonding, the TrkA inhibitory activity disappeared. This could be due to the fact that after the chain was replaced with a ring, the spatial conformation of the molecule was altered.

Design of Compounds with One-Chiral Atom. There are two chiral centers in LOXO-195 and TPX-0005, which posed great challenges for the synthesis and separation of such compounds. Compounds **7** and **8** were designed and synthesized, which contained only one chiral atom (Figure 3). Excitingly, both compounds had good inhibitory activity, particularly compound **8**, which showed a similar activity against wild TrkA/C with IC_{50} ranging from 0.2 to 3.2 nM to LOXO-195 and TPX-0005.

***In Vitro* PD and PK Data of Compound 8.** To determine the impact of TRK kinase resistance mutations on the activity of inhibitors, compound **8** was tested against purified kinase domains *in vitro*. Compound **8** achieved low nanomolar inhibitory activity against TrkA, $TrkA^{G595R}$, $TrkA^{G667C}$, TrkC, Alk, and Ros1, with IC_{50} values being 3.2, 2.1, 0.7, 0.2, 18.5, and 0.2 nM, respectively (Table 1). In an enzyme inhibition study, compound **8** also had good activity against mutant TrkA, especially its inhibitory activity against $TrkA^{G667C}$, which was 10−100 times higher than those of LOXO-195 and TPX-0005. The anti-tumor activity of compound **8** was evaluated using Ba/F3 cells, and the IC_{50} values were 0.2 and 5 nM in

https://doi.org/10.1021/acs.jmedchem.1c00712
J. Med. Chem. 2021, 64, 10286−10296

Table 2. PK Data of Compounds 8, 9, and 10 *In Vitro*

	LOXO-195	TPX-0005	8	9	10
cLog *P*	1.86	2.96	1.97	0.57	0.58
LLE[a]	6.3	5.6	6.5	7.7	8.0
$P_{appA\rightarrow B}$ (10^{-6} cm/s)/ER	8.4/4.1	0.9/45.3	16.3/1.4	3.9/9.5	12.0/2.8
KS[b] (μM)		65.8			192.9
MMS (mL/min/kg) H/R/M/D[c]	76/92/1351/38	29/49/982/21/	242/980/1010/268	43/29/342/74	17.7/28.8/1504/<10.7
PPB (Fu %) H/R/M/D	34/3/2/20	5/6/5/9	2/2/2/3	36/30/28/34	16/12/11/21
CYP (IC_{50}, μM): 1A2/2C9/2C19/2D6/3A4	>50/>50/>50/>50/>50	>50/6.4/12.3/28.5/>50			>100/18.1/89.0/>100/>50
hERG (IC_{50}, μM)				6.7	13

[a]LLE, ligand lipophilicity efficiency. [b]KS, kinetic solubility. [c]H/R/M/D, human/rat/mouse/dog.

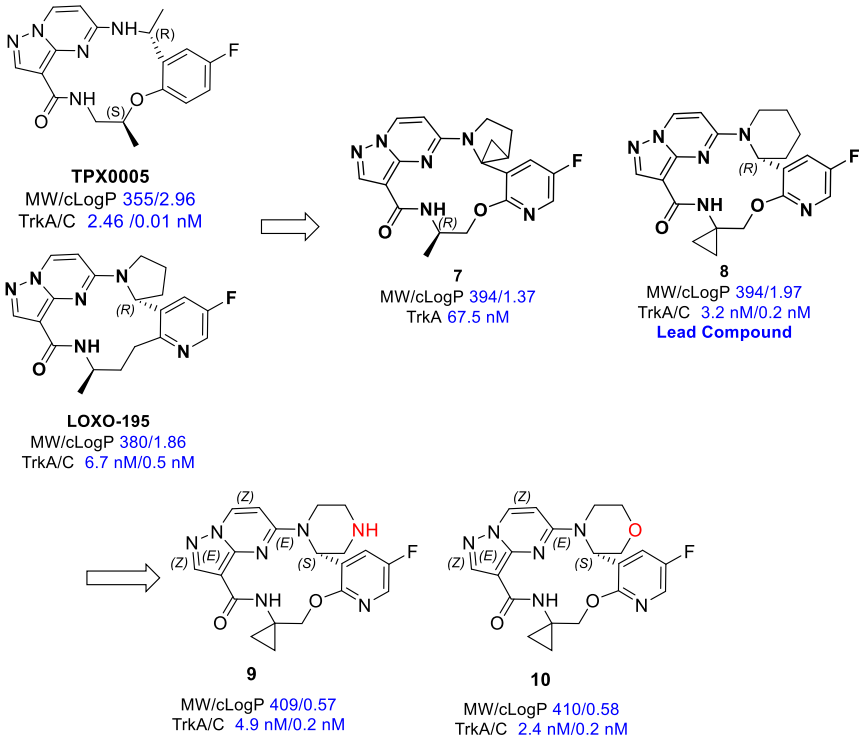

Figure 4. Design of compounds with one-chiral atom.

wild and mutant TrkA/C cells, respectively. In Ba/F3 cells with SLC34A2-Ros1 fusion, the activity of compound **8** was slightly lower (IC_{50} value: 12.6 nM).

Due to its good kinase inhibitory activity and cellular pharmacodynamics, the pharmacokinetic evaluation of compound **8** was carried out *in vitro* (Table 2). Most of the pharmacokinetic parameters of compound **8** were similar to those of LOXO-195 or TPX-0005 except for MMS (mL/min/kg). From the perspective of MMS, compound **8** was metabolized faster in humans, rats, and dogs. The oxidation on the piperidine ring may be the reason for the faster metabolism of compound **8**. Based on this finding, the structural optimization was continued.

***In Vitro* PD and PK Data of Compounds 9 and 10.** Substituting piperidine in compound **8** with piperazine gave compound **9** and replacing it with morpholine gave compound **10**. From the results of PD data *in vitro*, we can see that both compounds **9** and **10** maintained good inhibitory activity against WT and MT TrkA/TrkC, and IC_{50} values were essentially the same as those of compound **8** (Table 1). It is worth noting that the selectivity of compounds **9** and **10** to ALK was greatly improved, with IC_{50} values of 88.9 and 182.0 nM, respectively, while the IC_{50} value of compound **8** was 18.5 nM. This selectivity may be beneficial in reducing off-target side effects.

The pharmacokinetic evaluation of compounds **9** and **10** was carried out *in vitro* (Table 2). These results demonstrated that the drugability of compounds **9** and **10** was further improved compared to that of compound **8**. The ligand lipophilicity efficiencies (LLEs) of compounds **9** and **10** were 7.7 and 8.0, respectively, while the LLE of compound **8** was 6. The metabolic stability was greatly improved, and the MMS in humans, rats, and dogs were all less than 100 mL/min/Kg, which was not only superior to compound **8** but also better than LOXO-195 and TPX-0005. It was worth noting that the MMS values of these compounds in mice were significantly higher than those of other species, which may be caused by special metabolic enzymes. The inhibitory activity of compound **10** on the human ether-a-go-go-related gene (hERG) was much lower than that of compound **9**, with IC_{50} values of 13 and 6.7 μM, respectively. Therefore, compound **10** as a preclinical drug candidate continued to

https://doi.org/10.1021/acs.jmedchem.1c00712
J. Med. Chem. 2021, 64, 10286−10296

undergo efficacy and pharmacokinetic evaluation *in vivo* (Figure 4).

Kinase Assay Data of Compound 10. Kinase assays (Table 3) showed that compound **10** could inhibit the activities of TrkA, TrkB, and TRC with high selectivity at 0.5 μM (kinase activity remaining, <10%) and slightly inhibit the activities of ALK and ROS1 (kinase activity remaining, 10−30%), and the inhibitory activities of other kinases were not significantly affected by compound **10**.

Table 3. Kinase Assay Data of Compound 10

kinases	activity (% control)	kinases	activity (% control)
ALK	26	Met(M1268T)	86
A-Raf	103	Met(Y1248C)	85
Blk	46	Met(Y1248D)	96
BTK(R28H)	74	Met(Y1248H)	89
B-Raf	111	PDGFRα	106
B-Raf(V599E)	87	PDGFRα(D842V)	102
cKit	100	PDGFRα(V561D)	103
cKit(D816V)	101	Ret(h)	64
cKit(D816H)	96	Ret(V804L)	59
cKit(V560G)	109	Ret(V804M)	54
cKit(V654A)	105	RIPK1	102
c-RAF	103	RIPK2	93
EGFR	108	Ron	112
EGFR(L858R)	91	Ros1	16
EGFR(L861Q)	95	Src(1−530)	33
EGFR(T790M)	105	Src(T341M)	55
FAK	72	TrkA	2
FGFR1	92	TrkB	−1
FGFR2	93	TrkC	−3
FGFR3	96	JAK1	91
FGFR4	114	JAK2	44
Met	98	JAK3	94
Met(D1246H)	91	KDR	108

***In Vivo* PD and PK Data of Compound 10.** After a single intravenous administration of compound **10** at a dose of 2 mg/kg, the mean terminal half-life ($t_{1/2}$) was 0.87 h for male rats and 2.21 h for female rats. The exposure area under the curve (AUC_{0-t}) in female rats was significantly higher (2.5-fold) than that in male rats. After a single intragastric administration of 10 mg/kg, the time to peak (T_{max}) concentrations was 0.667 h. The AUC_{0-t} were 11,720 nM*h in male and 31,676 nM*h in female rats, respectively. The bioavailability was 56.0−61.9%.

Four engineered BaF3-NTRK xenograft tumor models were used to assess the therapeutic effect of compound **10** on tumor growth. Mice bearing 100−200 mm^3 tumors were treated orally at doses of 5, 10, or 20 mg/kg, once daily for 21 days. As shown in Figure 5, compound **10** produced significant inhibition of tumor growth both in wild-type NTRK fusion mutation cells (Ba/F3 LMNA-NTRK1cells and Ba/F3 ETV6-NTRK3 cells) and drug-resistant mutation cells (Ba/F3 ETV6-NTRK3-G623R cells and Ba/F3 LMNA-NTRK1-G595R) at all three doses, and the anti-tumor effect of compound **10** at 10 mg/kg was similar to that of LOXO-195 at 100 mg/kg. In addition, some side effects were observed in the LOXO-195 group, including unkempt appearance, weight loss, or even death. In contrast, animals that received the highest dose of compound **10** only showed slight weight loss and all animals survived during the treatment period. In our previous 4 weeks of repeated administration toxicity study in Cynomolgus monkeys, treatment-related changes included gait disturbance, impaired balance, and poor coordination, which could be attributed to excessive on-target Trk receptor inhibition. In addition, no significant changes in food consumption, electrocardiogram, blood pressure, hematological and biochemical parameters, organ weight, or bone marrow parameters were observed.[16] All these data suggest that compound **10** was more efficacious and safer against tumor growth than LOXO-195 (Table 4).

Chemistry. A typical synthetic route toward macrocyclic compound **10** is described in Scheme 1. Compound **10-1** was protected by Boc_2O (Boc, *tert*-butyloxycarbonyl) with *N*,*N*-dimethylpyridin-4-amine in THF to afford **10-2**. Enol phosphate **10-3** was synthesized from compound **10-2** by reaction with diphenyl phosphorochloridate under basic conditions in THF. Subsequent Suzuki−Miyaura coupling was performed with borate **10-4** to give **10-5**. Compound **10-5** was reduced with H_2 and $Pd(OH)_2/C$ in EtOH to afford **10-6**. Compound **10-7** was obtained from **10-6** *via* deprotection under acid conditions. Compounds **10-3**, **10-5**, **10-6**, and **10-7** did not need to be purified, and the crude product was directly subjected to the next reaction. Compound **10-7** was alkylated by ethyl 5-chloropyrazolo[1,5-a]pyrimidine-3-carboxylate **10-8** with *N*,*N*-diisopropylethylamine in NMP to afford **10-9**. Compound **10-9** was demethylated with chlorotrimethylsilane to obtain compound **10-10**, and the hydrolysis was continued to afford compound **11-11**. Compounds **10-11** and **10-12** were condensed with HATU to give compound **10-13**. After the intramolecular Mitsunobu reaction, compound **10-14** was obtained. The racemic material was purified by chiral chromatography to give the target compound **10**. As a result, compound **10** was found to be an R-isomer by single-crystal X-ray analysis, as shown in Figure 5.

CONCLUSIONS

Due to its high clinical efficacy, there is substantial interest in the development of small-molecule inhibitors of TrkA for the treatment of tumors. We have successfully discovered a novel, highly potent, and selective second-generation Trk inhibitor compound **10** (LPM4870108). Although initial efforts using a structural modification strategy was largely futile, compound **10** was found *via* optimization from the aspects of chemistry and pharmacokinetic properties, which had good activity against wild-type and mutant TrkA/TrkC. Moreover, the high potency, high off-target selectivity, good *in vivo* toxicity profile, as well as good absorption and human CL predictions made compound **10** an exciting and promising structurally differentiated asset suitable for advancement into a variety of clinical anti-tumor studies (Figure 6).

EXPERIMENTAL SECTION

General. The recorded ^1H nuclear magnetic resonance (NMR) spectra were found to be consistent with the proposed structures. Characteristic chemical shifts (δ) are given in parts-per-million (ppm) (δ relative to the residual solvent peak) using conventional abbreviations for the designation of major peaks: s, singlet; d, doublet; t, triplet; m, multiplet; and br, broad. The mass spectra (m/z) were recorded using the electrospray ionization technique. The following abbreviations were used for common solvents: $CDCl_3$, deuterochloroform; DMSO-d_6, deuterodimethyl sulfoxide; and CD_3OD, deuteromethanol. All solvents were of reagent grade and, when necessary, were purified and dried by standard methods. The concentration of solutions after reactions and extractions involved the

https://doi.org/10.1021/acs.jmedchem.1c00712
J. Med. Chem. 2021, 64, 10286−10296

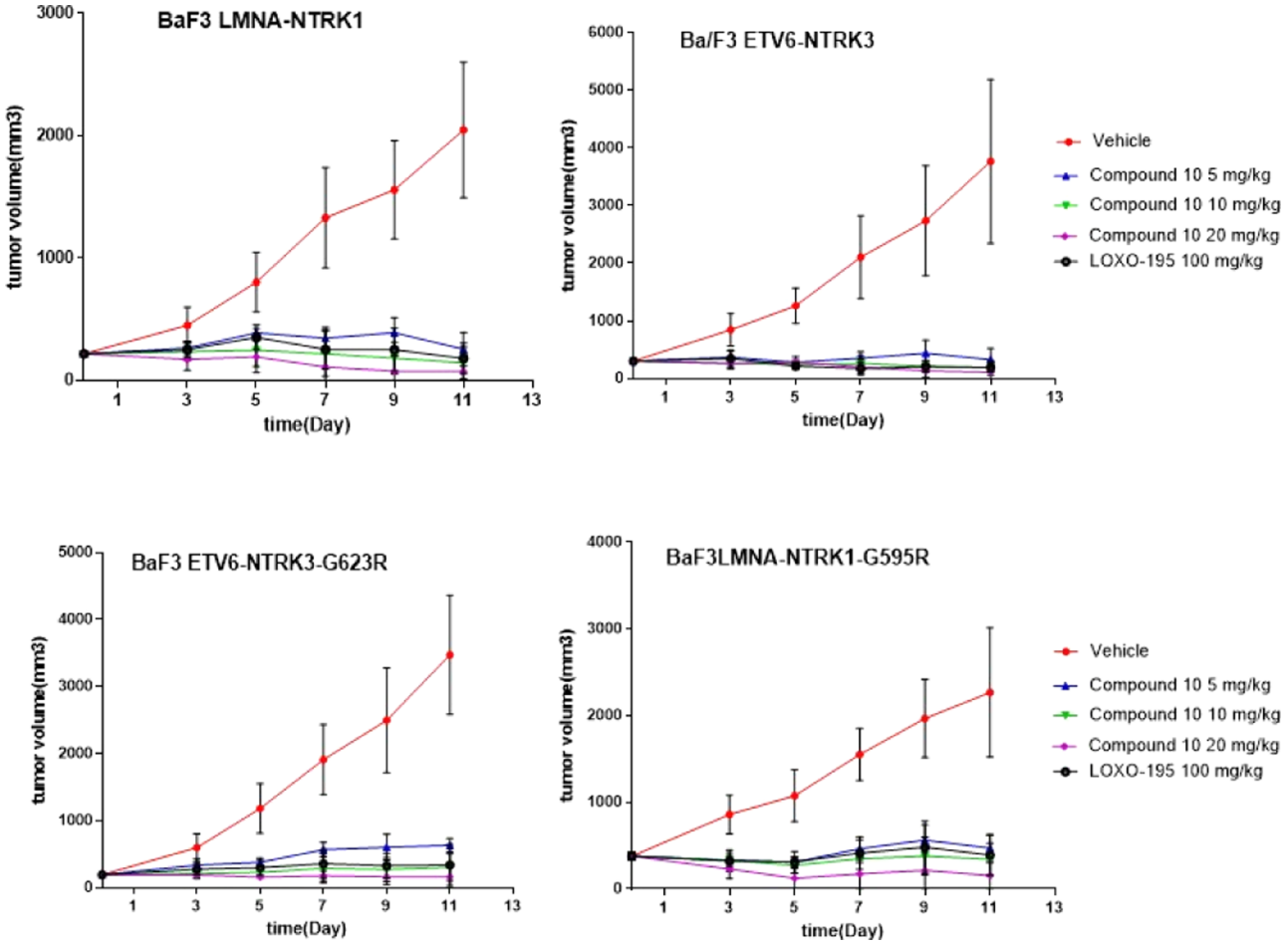

Figure 5. *In vivo* efficacy of compound **10** against four engineered BaF3-NTRK tumor models.

Table 4. PK Data of Compound 10 in Sprague–Dawley Rats

	LOXO-195	TPX-0005	**10**	
dose (mpk)	3	3	2 (M)	2 (F)
C_0 (nM)	23,779 ± 1526	12,870 ± 831	4118 ± 833	3509 ± 719
$T_{1/2}$ (h)	1.2 ± 0.1	2.8 ± 0.1	0.872 ± 0.0156	2.21 ± 0.215
V_d (L/kg)	0.5 ± 0.1	1.1 ± 0.2	1.39 ± 0.229	1.46 ± 0.224
Cl (mL/kg/min)	11.8 ± 0.8	9.4 ± 0.5	19.3 ± 0.624	8.19 ± 1.96
AUC_{0-t} (nM*h)	11,146 ± 656	15,002 ± 859	4191 ± 139	10,282 ± 2298
dose (mpk)	10	10	10 (M)	10 (F)
C_{max} (nM)	12,700 ± 1121	16,900 ± 1173	6384 ± 1525	6628 ± 626
T_{max} (h)	0.4 ± 0.0	0.8 ± 0.0	0.667 ± 0.289	0.667 ± 0.289
AUC_{0-t} (nM*h)	27,344 ± 1590	59,724 ± 1434	11,720 ± 1749	31,676 ± 6628
F %	74 ± 3	119 ± 4	56.0 ± 8.4	61.9 ± 13.0

use of a rotary evaporator operating at a reduced pressure of *ca.* 20 Torr. Anhydrous solvents were obtained from commercial sources and used as received. The chemical yields reported below are unoptimized. Purity criteria: final compounds isolated as singletons are >95% based on LCMS and/or HPLC.

*tert-Butyl 3-Oxomorpholine-4-carboxylate (**10-2**).* 4-Dimethylaminopyridine (12.08 g, 98.91 mmol, 0.1 equiv) was added to the solution of compound **10-1** (morpholin-3-one) (100 g, 989.08 mmol, 1 equiv) in tetrahydrofuran (1000 mL) and then Boc_2O (280.62 g, 1.29 mol, 295.39 mL, 1.3 equiv) was dropped. The mixture was stirred at 30 °C for 2 min and poured into an aqueous sodium chloride solution (1 L). The reaction was extracted with EtOAc. The combined organic phases were added with 1% HCl to adjust the pH to 5–6 in an ice bath, washed with water, dried over Na_2SO_4, filtered, and concentrated to obtain compound **10-2** (185 g, crude product) as a yellow oily compound.

*tert-Butyl 5-((Diphenoxyphosphoryl)oxy)-2,3-dihydro-4H-1,4-oxazine-4-carboxylate (**10-3**).* Under nitrogen, LiHMDS (1 M, 546.67 mL, 1 equiv) was slowly dropped into the solution of compound **10-2** (110 g, 546.67 mmol, 1 equiv) in tetrahydrofuran (1000 mL) and the temperature of the reaction was controlled between −60 and −30 °C. The reaction mixture was stirred for 1 h and then diphenyl chlorophosphate (146.85 g, 546.67 mmol, 112.96 mL, 1 equiv) in tetrahydrofuran (120 mL) was added dropwise. After stirring for 3 h, the reaction mixture was poured into water (1000 mL) and extracted with EtOAc. The organics were washed with water, dried over Na_2SO_4, filtered, and concentrated. The crude material was purified by SiO_2 column chromatography to afford **10-3** (127 g, 293.3 mmol, yield 52.87%).

https://doi.org/10.1021/acs.jmedchem.1c00712
J. Med. Chem. 2021, 64, 10286–10296

Scheme 1. Synthetic Route for Compound 10[a]

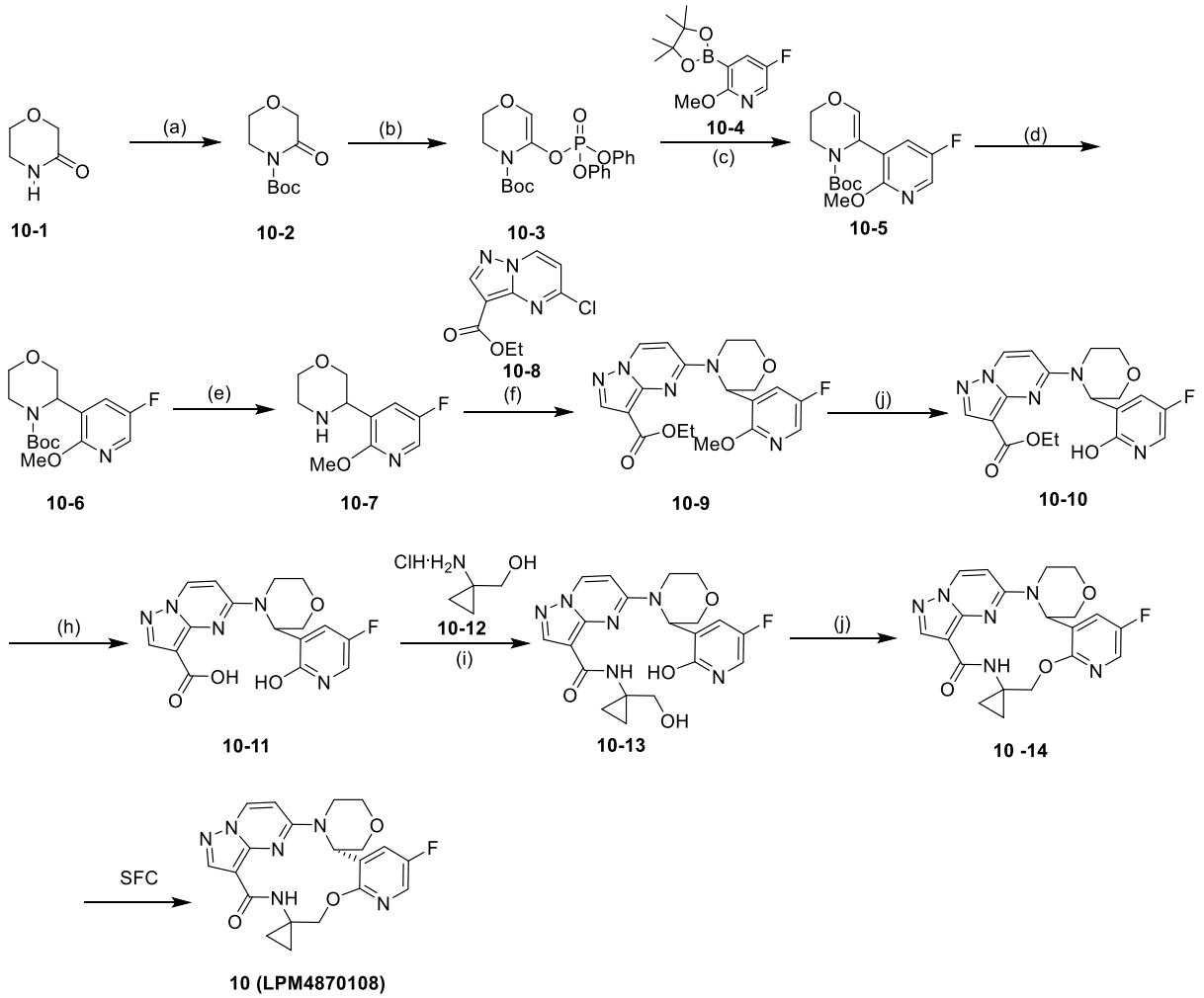

[a]Reagents and conditions: (a) Boc_2O, DMAP, THF, RT, 16 h, 93%; (b) $ClPO(OPh)_2$, LiHMDS, THF; (c) $Pd(PPh_3)_4$, $NaHCO_3$, THF/H_2O, reflux, 16 h; (d) H_2, $Pd(OH)_2/C$ (5% wt), EtOH, 96 h; (e) HCl/EA, the total yield is 44% from step b to e; (f) DIPEA, NMP, 75 °C, 16 h, 85.3%; (g) TMSCl, NaI, ACN, 75 °C, 2 h; (h) NaOH, H_2O/MeOH, 60 °C, 2 h, total yield of steps g and h is 98.6%; (i) HATU, DIPEA, DMF, RT, 72.4%; (j) PPh_3, DEAD, THF.

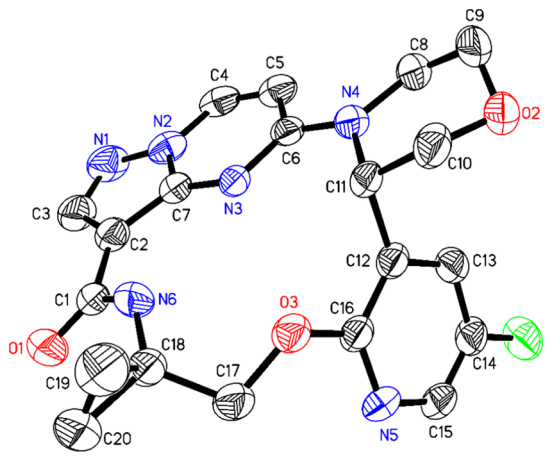

Figure 6. ORTEP of **10**.

*tert-Butyl 5-(5-Fluoro-2-methoxypyridin-3-yl)-2,3-dihydro-4H-1,4-oxazine-4-carboxylate (**10-5**).* Acetonitrile (1000 mL), water (250 mL), compound **10-3** (70 g, 161.52 mmol, 1 equiv), potassium phosphate (68.57 g, 323.04 mmol, 2 equiv), and compound **10-4** (81.75 g, 323.04 mmol, 2 equiv) were sequentially added to the flask. After nitrogen replacement, tri-*tert*-butylphosphine palladium (6 g, 11.74 mmol) was added under a nitrogen flow, and the reaction mixture was heated at 75 °C for 10 h. The reaction mixture was poured into water (1000 mL) and extracted with EtOAc. The organics were washed with water, dried over Na_2SO_4, filtered, and concentrated. The crude material was purified by SiO_2 column chromatography to afford **10-5** (39.6 g, 127.8 mmol, yield 78.9%). LCMS [M + 1] 311.1; ^{1}H NMR (400 MHz, chloroform-*d*): δ ppm 7.87 (d, J = 2.8 Hz, 1H), 7.24–7.19 (m, 1H), 6.30–6.22 (m, 1H), 4.26–4.19 (m, 2H), 3.90 (s, 3H), 3.83–3.75 (m, 2H), 1.15 (s, 9H).

*tert-Butyl 3-(5-Fluoro-2-methoxypyridin-3-yl)morpholine-4-carboxylate (**10-6**).* Compound **10-5** (30 g, 96.67 mmol, 1 equiv) was dissolved in ethanol (1000 mL) and then dry palladium hydroxide on carbon (9.62 g, 13.69 mmol, 20% purity) was added under an argon atmosphere. Under a hydrogen atmosphere (50 psi), the reaction was heated at 80 °C for 24 h. The reaction solution was filtered, and the filter cake was washed with ethanol (50 mL). The filtration was concentrated in vacuo to obtain compound **10-6** as a white solid (27.8 g, 89.1 mmol, yield 91.95%). LCMS [M + 1] 313.2; ^{1}H NMR (400 MHz, chloroform-*d*): δ ppm 7.87 7.83 (d, J = 2.8 Hz, 1H), 7.24 (dd, J = 2.4, 8.7 Hz, 1H), 5.06 (br d, J = 3.8 Hz, 1H), 4.19 (br d, J = 12.0 Hz, 1H), 3.91–3.79 (m, 5H), 3.72 (dd, J = 4.3, 12.0 Hz, 1H), 3.51 (dt, J = 3.4, 11.6 Hz, 1H), 3.36–3.23 (m, 1H), 1.33 (s, 9H).

https://doi.org/10.1021/acs.jmedchem.1c00712
J. Med. Chem. 2021, 64, 10286–10296

*3-(5-Fluoro-2-methoxypyridin-3-yl)morpholine (**10-7**).* HCl/ethyl acetate (4 M, 750.69 mL, 10.91 equiv) was added to the solution of compound **10-6** (86 g, 275.34 mmol, 1 equiv) in ethyl acetate (300 mL), and the reaction mixture was stirred at 25 °C for 16 h. A large amount of white solid precipitated. Under a nitrogen atmosphere, the reaction solution was filtered, washed with ethyl acetate (300 mL), and the filter cake was vacuum-dried without further purification to obtain compound **10-7** as a white solid (57.46 g, 271 mmol, yield 98.33%). LCMS [M + 1] 213.1; ^{1}H NMR (400 MHz, chloroform-*d*): δ ppm 7.88 (d, J = 3.0 Hz, 1H), 7.62−7.57 (m, 1H), 4.17 (dd, J = 3.0, 9.2 Hz, 1H), 3.96 (dd, J = 3.2, 10.8 Hz, 1H), 3.92 (s, 3H), 3.89−3.84 (m, 1H), 3.61 (dt, J = 2.6, 11.0 Hz, 1H), 3.24 (dd, J = 9.2, 10.4 Hz, 1H), 3.15−3.06 (m, 1H), 3.03−2.96 (m, 1H).

*Ethyl 5-(3-(5-Fluoro-2-methoxypyridin-3-yl)morpholino)-pyrazolo[1,5-a]pyrimidine-3-carboxylate (**10-9**).* *N*,*N*-Diisopropylethylamine (88.09 g, 681.58 mmol, 118.72 mL, 2.53 equiv) and compound **10-8** (50.37 g, 223.24 mmol, 0.83 equiv) were added to the mixture of compound **10-7** (67 g, 269.42 mmol, 1 equiv, HCl) in 1-methyl-2-pyrrolidone (350 mL) and then stirred at 70 °C for 16 h. The reaction solution was poured into ice water (1000 mL) and stirred for 30 min. A large number of solids precipitated out, which were then filtered and washed with water (400 mL). The filter cake was dissolved in dichloromethane (1.5 L), dried with anhydrous sodium sulfate, and concentrated in vacuo to obtain compound **10-9** (92.2 g, crude product, yield 85.33%).

*Ethyl 5-(3-(5-Fluoro-2-hydroxypyridin-3-yl)morpholino)-pyrazolo[1,5-a]pyrimidine-3-carboxylate (**10-10**).* The crude compound **10-9** (90 g, 224.77 mmol, 1 equiv) was dissolved in the acetonitrile solvent (900 mL), then sodium iodide (101.08 g, 674.32 mmol, 3 equiv) and trimethylchlorosilane (73.26 g, 674.32) mmol, 85.58 mL, (3 equiv) were added, and the reaction solution was stirred at 25 °C for 24 h. The reaction solution was poured into an aqueous sodium bicarbonate solution (prepared with 65 g of sodium bicarbonate and 1.2 L of water), then the pH was adjusted to 7−8, and extracted with dichloromethane (500 mL). The organic phase was washed with saturated sodium chloride (150 mL), dried over anhydrous sodium sulfate, and concentrated in vacuo to obtain a crude product. The crude product was slurried (ethyl acetate−methyl *tert*-butyl ether = 1:1, 400 mL) for 1 h, filtered, and the filter cake was dried in vacuo to obtain compound **10-10** as a pale yellow solid (86 g, crude product).

*5-(3-(5-Fluoro-2-hydroxypyridin-3-yl)morpholino)pyrazolo[1,5-a]pyrimidine-3-carboxylic Acid (**10-11**).* Compound **10-10** (85 g, 219.43 mmol, 1 equiv) was dissolved in methanol and then sodium hydroxide (3 M, 292.58 mL, 4 equiv), water (292 mL), and methanol (850 mL) were added. The reaction mixture was stirred at 60 °C for 2 h. After the reaction mixture was cooled in an ice water bath, 3 mol/L dilute hydrochloric acid was slowly added to adjust the pH to 2. After stirring for 0.5 h, a solid precipitated out. It was filtered and the filter cake was dried in concentrated vacuum to obtain compound **10-11** as a light brown solid (60.5 g, 168.38 mmol, yield 76.73%). LCMS [M + 1] 360.9; ^{1}H NMR (400 MHz, DMSO-d_6): δ ppm 11.75 (br s, 1H), 8.74 (d, J = 8.0 Hz, 1H), 8.21 (s, 1H), 7.56 (br s, 1H), 7.44 (br d, J = 8.0 Hz, 1H), 6.72 (br d, J = 8.0 Hz, 1H), 5.31 (br s, 1H), 4.51 (br s, 1H), 4.37 (br d, J = 12.0 Hz, 1H), 4.07 (br d, J = 8.4 Hz, 1H), 3.84 (br dd, J = 4.0, 11.8 Hz, 1H), 3.66−3.45 (m, 3H).

*5-(3-(5-Fluoro-2-hydroxypyridin-3-yl)morpholino)-N-(1-(hydroxymethyl)cyclopropyl)pyrazolo[1,5-a]pyrimidine-3-carboxamide (**10-13**).* Compound **10-11** (53.5 g, 148.90 mmol, 1 equiv) and compound **10-12** (20.24 g, 163.79 mmol, 1.1 equiv) were dissolved in *N*,*N*-dimethylformamide (530 mL) and then 2-(7-benzotriazole oxide)-*N*,*N*,*N*′,*N*′-tetramethylurea hexafluorophosphate (62.28 g, 163.79 mmol, 1.1 equiv) was added. After *N*,*N*-diisopropyl ethylamine (67.35 g, 521.14 mmol, 90.77 mL, 3.5 equiv) was added dropwise and the reaction solution was heated at 15 °C for 16 h. The reaction was quenched by adding 16 mL of saturated aqueous ammonium chloride solution to the reaction solution and concentrated in vacuo at 60 °C. After concentration, acetonitrile (400 mL) was added and it was stirred for 1 h. A large amount of solids precipitated. This solid was filtered to obtain compound **10-13** (72 g). LCMS [M + 1] 429.1; ^{1}H NMR (400 MHz, DMSO-d_6): δ ppm 8.80 (d, J = 8.0 Hz, 1H), 8.15 (s, 1H), 7.87 (s, 1H), 7.56 (s, 1H), 7.43 (d, J = 6.4 Hz, 1H), 6.81 (s, 1H), 5.38 (s, 1H), 4.69 (s, 1H), 4.31 (d, J = 19.2 Hz, 1H), 4.22 (s, 1H), 4.08−4.02 (m, 2H), 3.89−3.85 (m, 2H), 3.66 (d, J = 6.8 Hz, 3H), 0.75−0.71 (m, 3H), 0.60 (br s, 1H).

*(3′*E*,4′*E*)-5′-Fluorospiro[cyclopropane-1,6′-4-oxa-7-aza-2(4,3)-morpholina-1(5,3)-pyrazolo[1,5-a]pyrimidina-3(3,2)-pyridinacyclooctaphan]-8′-one (**10-14**).* Compound **10-13** (25 g, 58.35 mmol, 1 equiv) was dissolved in tetrahydrofuran (250 mL), then tributylphosphorus (17.71 g, 87.53 mmol, 21.60 mL, 1.5 equiv) was added dropwise, followed by azodimethyl bis(piperidine) (22.09 g, 87.53 mmol, 1.5 equiv), and it was stirred at 15 °C for 16 h. The reaction solution was directly filtered, and the obtained white filter cake was compound **10-14** (35 g, crude product). The crude product was dissolved in dichloromethane (1000 mL) and methanol (100 mL), washed twice with 1 M HCl (250 mL), the organic phase was dried and concentrated in vacuo to obtain the crude product. The crude product was slurried with ethanol (500 mL) and stirred for 1 h, filtered, and the filter cake was vacuum-dried to obtain compound **10-14** (22 g). LCMS [M + 1] 411.1; ^{1}H NMR (400 MHz, $CDCl_3$): δ ppm 8.98 (s, 1H), 8.33 (d, J = 7.6 Hz, 1H), 8.26 (s, 1H), 7.89 (d, J = 2.4 Hz, 1H), 7.77−7.75 (m, 1H), 6.36 (d, J = 7.6 Hz, 1H), 6.15 (s, 1H), 5.07 (d, J = 10.8 Hz, 1H), 4.39 (d, J = 9.6 Hz, 1H), 4.12−3.88 (m, 4H), 3.76 (d, J = 10.0 Hz, 1H), 3.60 (d, J = 10.8 Hz, 1H), 2.27−2.22 (m, 1H), 1.07−0.94 (m, 2H), 0.84−0.79 (m, 1H).

*(S,3′*E*,4′*E*)-5′-Fluorospiro[cyclopropane-1,6′-4-oxa-7-aza-2(4,3)-morpholina-1(5,3)-pyrazolo[1,5-a]pyrimidina-3(3,2)-pyridinacyclooctaphan]-8′-one (**10**).* Column: CHIRALPAK IG-3 (IG30CD-WE016), 0.46 cm ID × 15 cm L; mobile phase: MeOH/DCM = 60/40 (V/V); flow rate: 1.0 mL/min; wavelength: UV 220 nm; Temperature: 35 °C; HPLC equipment: Shimadzu LC-20AT CP-HPLC-06. LCMS [M + 1] 411.1; ^{1}H NMR (400 MHz, $CDCl_3$): δ ppm 8.98 (s, 1H), 8.33 (d, J = 7.6 Hz, 1H), 8.26 (s, 1H), 7.89 (d, J = 2.4 Hz, 1H), 7.77−7.75 (m, 1H), 6.36 (d, J = 7.6 Hz, 1H), 6.15 (s, 1H), 5.07 (d, J = 10.8 Hz, 1H), 4.39 (d, J = 9.6 Hz, 1H), 4.12−3.88 (m, 4H), 3.76 (d, J = 10.0 Hz, 1H), 3.60 (d, J = 10.8 Hz, 1H), 2.27−2.22 (m, 1H), 1.07−0.94 (m, 2H), 0.84−0.79 (m, 1H). ^{13}C NMR (100 MHz, $CDCl_3$): δ ppm 163.47, 157.17, 156.25, 155.36, 146.03, 145.60, 138.58, 132.71, 125.85, 125.06, 103.55, 96.29, 75.25, 70.91, 66.09, 46.33, 42.40, 33.55, 11.91, 8.29. HRMS for $C_{20}H_{20}FN_6O_3$ m/z: $[M+H]^+$ calcd, 411.15754; found, 411.15746. HPLC 99.64%, chiral HPLC 98.84%.

Computational Modeling Methods. All molecules were prepared for docking simulation using Discovery Studio 2018 to consider proper protonation states and tautomers. The docking simulation was performed with CDOCK (Discovery Studio 2018) using protein models based on X-ray structures (PDB ID: 4YNE) downloaded from RCSB PDB (http://www.rcsb.org/).

Permeability Experiment. A permeability experiment was conducted with the Caco-2 cell model. Caco-2 cells were seeded on 96-well transport inserts and cultured for 28 days before being used for the experiment. The apical-to-basolateral (A to B) transport of the test compound was measured by adding a transport buffer solution (HBSS, 25 mM HEPES, pH 7.4) containing the test compound (or rosuvastatin or propranolol as the control) to the apical and transport buffer solution (HBSS, 25 mM HEPES, pH 7.4) to basolateral. The basolateral-to-apical (B to A) transport of the test compound was measured by adding transport buffer solution (HBSS, 25 mM HEPES, pH 7.4) containing the test compound to the basolateral and transport buffer solution (HBSS, 25 mM HEPES, pH 7.4) to apical. After incubating at 37 °C for 2 h, the cell plates were taken out and samples on both sides were obtained. The concentrations of the test compound were determined by LC−MS/MS. According to the concentrations of the substrate at the donor compartment and the receiver compartment, the apparent permeability of substrate transport from the apical to the basolateral and from the basolateral to the apical in the monolayer were calculated, and the efflux ratio was calculated.

https://doi.org/10.1021/acs.jmedchem.1c00712
J. Med. Chem. 2021, 64, 10286−10296

Metabolism Stability in Microsomes. The test compound was incubated in liver microsomes at a final concentration of 1 μM, and the protein concentration was 0.5 mg mL^{-1}. The reactions were terminated at serial time points after initiation of the reaction. The test compound was analyzed using an optimized LC−MS/MS method. The percentages of the remaining test compound were measured and the *in vitro* intrinsic clearance was calculated accordingly. Hepatic intrinsic clearance ($CL_{int,\ in\ vivo}$) was evaluated based on the *in vitro* intrinsic clearance.

Plasma Protein Binding Assay. Plasma protein binding studies were performed using a 96-well HTDialysis equilibrium dialysis chamber apparatus. Spiked plasma and phosphate buffer were added to the donor side and the receiver side, respectively. The plate was covered with an adhesive sealing film and placed in a water bath at 37 °C with shaking. After a certain time, the samples in the donor side and the receiver side were taken out and analyzed using an optimized LC−MS/MS method. The values of unbound fraction (fu) were calculated.

CYP Isoenzyme Inhibition Experiment. Serial concentrations of the test compound were incubated with each probe substrate (phenacetin for CYP1A2, diclofenac for CYP2C9, S-mephenytoin for CYP2C19, dextromethorphan for CYP2D6, and midazolam and testosterone for CYP3A4) in pooled human liver microsomes. The reaction was initiated by the addition of the coenzyme NADPH. The reaction was stopped by adding the ice-cold acetonitrile-containing internal standard to the incubation system. The generation amounts of probe drug metabolites (acetaminophen, OH-diclofenac, OH-S-mephenytoin, dextrorphan, OH-midazolam, and 6-OH-testosterone) at different test compound concentrations were measured by the LC−MS/MS method to calculate the remaining activity percentage of liver microsomal enzymes, and finally the IC_{50} values of test compounds for the cytochrome P450 (CYP) isoenzyme were obtained using Graphpad Prism 6.02 software. Selective inhibitors (α-naphthoflavone for CYP1A2, sulfaphenazole for CYP2C9, nootkatone for CYP2C19, quinidine for CYP2D6, and ketoconazole for CYP3A) were used as the positive controls to validate the incubation system.

Kinase Assay. Compound **10** was tested against each of the selected kinases using Eurofins standard KinaseProfiler assays. The compounds supplied were prepared to a working stock of 50× final assay concentration in 100% DMSO. The required volume of the 50× stock of the test compound was added to the assay well before a reaction mix containing the enzyme and the substrate was added. The reaction was initiated by the addition of ATP at the selected concentration. Data were handled using custom-built in-house analysis software. The results were expressed as kinase activity remaining, as a percentage of the DMSO control, which were calculated using the following formula (mean of sample counts − mean of blank counts)/mean of control counts.

***In Vitro* PD Assay.** The indicated kinases (TrkA, $TrkA^{G595R}$, $TrkA^{G667C}$, TrkC, ALK, or Ros1) were delivered into the substrate solution and gently mixed. Then, the compounds in DMSO were delivered to the kinase reaction mixture utilizing the acoustic technology (Echo 550). ^{33}P-ATP (specific activity, 0.01 μCi/μL final) was added to the reaction mixture to initiate the reaction. The kinase reaction was incubated for 120 min at room temperature. Reactions were spotted onto P81 ion-exchange paper (Whatman # 3698-915). The filters were washed extensively in 0.75% phosphoric acid. The radioactive phosphorylated substrate remaining on the filter paper was measured. Kinase activity data were expressed as the percent remaining kinase activity in the test samples compared to vehicle (dimethyl sulfoxide) reactions. IC_{50} values and curve fits were obtained using GraphPad Prism 5.

The cell viability was evaluated using the cytotoxicity assay, as described previously.[17] Briefly, cells were plated at 5000 per well into 96-well plates and then incubated with compounds **8**−**10** at the desired concentrations. The MTT solution (5 mg/mL) was added to each well and incubated continuously for 4 h. DMSO was added to dissolve the MTT formazan product, and the absorbance was measured at 570 nm using a Molecular Devices SpectraMax M5 (Molecular Devices, USA). IC_{50} values were calculated using GraphPad Prism 5.

***In Vivo* PD Study.** Animals were provided free access to food and water in strict accordance with the National Institute of Health Guide for the Care and Use of Laboratory Animals (NIH Publications no. 80-23). All animal protocols were approved by the Ethics Committee of Yantai University (no. 011 in 2020 for Animal Ethics Approval). All surgeries were performed under anesthesia, and all efforts were made to minimize suffering. Twelve Sprague−Dawley rats (six males and six females) were divided into two groups (three males and three females) randomly. Animals in group A were administered with the test compound by single intravenous administration at 2 mg/kg. Animals in group B were administered with the test compound by single oral administration at 10 mg/kg. Blood samples were collected from the jugular vein cannula at a pre-dose, and 0.083, 0.25, 0.5, 1, 2, 4, 6, 8, 12, and 24 h after finishing the dose for group A and collected at pre-dose and 0.25, 0.5, 1, 2, 4, 6, 8, 12, and 24 h after finishing the dose for group B. The concentration of the test compound was analyzed using an optimized LC−MS/MS method. The pharmacokinetic (PK) parameters were calculated using a non-compartmental model of WinNonlin version 8.0 (Pharsight, St. Louis, USA).

Xenograft models (eight animals/group) were established following a subcutaneous injection of 3×10^6 Ba/F3 LMNA-NTRK1cells, Ba/F3 ETV6-NTRK3 cells, Ba/F3 ETV6-NTRK3-G623R cells, or Ba/F3 LMNA-NTRK1-G595R cells into the right flank of each animal. When tumors in all animals ranged from 100 to 200 mm^3 in size, compound **10** was administered orally once daily for 11 days at doses of 5, 10, or 20 mg/kg, and LOXO-195 was administered at 100 mg/kg, respectively. Tumor dimensions and body weights were recorded twice weekly starting from the first day of treatment, and tumor volumes were calculated using the formula $(l \times (w)^2)/2$, where l was the longest dimension of the tumor and w was the width, respectively.

■ ASSOCIATED CONTENT

Supporting Information

The Supporting Information is available free of charge at https://pubs.acs.org/doi/10.1021/acs.jmedchem.1c00712.

Crystallographic data of compounds (CSV)

^{1}H NMR, ^{13}C NMR, COSY, HSQC, HMBC, ^{19}F NMR, HRMS, and single-crystal X-ray diffraction experiment report of compound **10** (PDF)

Predicted binding mode of LOXO-195 and TPX-0005 binding to the active site of TrkC (PDF)

■ AUTHOR INFORMATION

Corresponding Authors

Hongbo Wang − *School of Pharmacy, Key Laboratory of Molecular Pharmacology and Drug Evaluation (Yantai University), Ministry of Education, Collaborative Innovation Center of Advanced Drug Delivery System and Biotech Drugs in Universities of Shandong, Yantai University, Yantai 264005, China*; orcid.org/0000-0001-5055-4261; Phone: 86-535-6706060; Email: hongbowangyt@gmail.com

Jingwei Tian − *School of Pharmacy, Key Laboratory of Molecular Pharmacology and Drug Evaluation (Yantai University), Ministry of Education, Collaborative Innovation Center of Advanced Drug Delivery System and Biotech Drugs in Universities of Shandong, Yantai University, Yantai 264005, China*; Email: tianjingwei@luye.cn

Authors

Zongliang Liu − *School of Pharmacy, Key Laboratory of Molecular Pharmacology and Drug Evaluation (Yantai University), Ministry of Education, Collaborative Innovation Center of Advanced Drug Delivery System and Biotech Drugs*

in Universities of Shandong, Yantai University, Yantai 264005, China

Pengfei Yu − *Department of Clinical Medicine, Binzhou Medical College, Yantai 256603, China*

Lin Dong − *Luye Pharma Group, Yantai 264005, China*

Wenyan Wang − *School of Pharmacy, Key Laboratory of Molecular Pharmacology and Drug Evaluation (Yantai University), Ministry of Education, Collaborative Innovation Center of Advanced Drug Delivery System and Biotech Drugs in Universities of Shandong, Yantai University, Yantai 264005, China*

Sijin Duan − *Luye Pharma Group, Yantai 264005, China*

Bingsi Wang − *Luye Pharma Group, Yantai 264005, China*

Xiaoyan Gong − *Luye Pharma Group, Yantai 264005, China*

Liang Ye − *Department of Clinical Medicine, Binzhou Medical College, Yantai 256603, China*

Complete contact information is available at: https://pubs.acs.org/10.1021/acs.jmedchem.1c00712

Author Contributions

Z.L. and P.Y. contributed equally. H.W. and J.T. designed the research. Z.L., P.Y., L.D., W.W., S.D., B.W., X.G., and L.Y. performed the experiments. H.W., J.T., and L.Y. performed data analyses. H.W. and J.T. wrote the paper.

Funding

This work was partially supported by grants from the National Natural Science Foundation of China (82073888), the Science and Technology Support Program for Youth Innovation in Universities of Shandong (2019KJM009 and 2020KJM003), The Medical and Health Science and Technology Development plan project of Shandong (2017WS691), the Top Talents Program for One Case Discussion of Shandong Province, and the Taishan Scholar Project.

Notes

The authors declare no competing financial interest.

■ ABBREVIATIONS

ATP, adenosine triphosphate; Boc, *tert*-butyloxycarbonyl; CYP, cytochrome P450; ER, efflux ratio; *F*, oral bioavailability; hERG, human ether-a-go-go-related gene; IC_{50}, half-maximum inhibitory concentration; MW, molecular weight; PDB, Protein Data Bank; PK, pharmacokinetics; $T_{1/2}$, half-life; Trk, tropomyosin-related kinase; V_d, volume of distribution at steady state

■ REFERENCES

(1) Mitelman, F.; Johansson, B.; Mertens, F. The impact of translocations and gene fusions on cancer causation. *Nat. Rev. Cancer* **2007**, *7*, 233−245.

(2) Drilon, A.; Laetsch, T. W.; Kummar, S.; DuBois, S. G.; Lassen, U. N.; Demetri, G. D.; Nathenson, M.; Doebele, R. C.; Farago, A. F.; Pappo, A. S.; Turpin, B.; Dowlati, A.; Brose, M. S.; Mascarenhas, L.; Federman, N.; Berlin, J.; El-Deiry, W. S.; Baik, C.; Deeken, J.; Boni, V.; Nagasubramanian, R.; Taylor, M.; Rudzinski, E. R.; Meric-Bernstam, F.; Sohal, D. P. S.; Ma, P. C.; Raez, L. E.; Hechtman, J. F.; Benayed, R.; Ladanyi, M.; Tuch, B. B.; Ebata, K.; Cruickshank, S.; Ku, N. C.; Cox, M. C.; Hawkins, D. S.; Hong, D. S.; Hyman, D. M. Efficacy of Larotrectinib in TRK Fusion-Positive Cancers in Adults and Children. *N. Engl. J. Med.* **2018**, *378*, 731−739.

(3) Amatu, A.; Sartore-Bianchi, A.; Siena, S. NTRK gene fusions as novel targets of cancer therapy across multiple tumour types. *ESMO Open* **2016**, *1*, No. e000023.

(4) Shah, N.; Lankerovich, M.; Lee, H.; Yoon, J.-G.; Schroeder, B.; Foltz, G. Exploration of the gene fusion landscape of glioblastoma using transcriptome sequencing and copy number data. *BMC Genom.* **2013**, *14*, 818.

(5) Greco, A.; Miranda, C.; Pierotti, M. A. Rearrangements of NTRK1 gene in papillary thyroid carcinoma. *Mol. Cell. Endocrinol.* **2010**, *321*, 44−49.

(6) Vaishnavi, A.; Le, A. T.; Doebele, R. C. TRKing down an old oncogene in a new era of targeted therapy. *Cancer Discovery* **2015**, *5*, 25−34.

(7) Vaishnavi, A.; Capelletti, M.; Le, A. T.; Kako, S.; Butaney, M.; Ercan, D.; Mahale, S.; Davies, K. D.; Aisner, D. L.; Pilling, A. B.; Berge, E. M.; Kim, J.; Sasaki, H.; Park, S.-i.; Kryukov, G.; Garraway, L. A.; Hammerman, P. S.; Haas, J.; Andrews, S. W.; Lipson, D.; Stephens, P. J.; Miller, V. A.; Varella-Garcia, M.; Jänne, P. A.; Doebele, R. C. Oncogenic and drug-sensitive NTRK1 rearrangements in lung cancer. *Nat. Med.* **2013**, *19*, 1469−1472.

(8) Ardini, E.; Bosotti, R.; Borgia, A. L.; De Ponti, C.; Somaschini, A.; Cammarota, R.; Amboldi, N.; Raddrizzani, L.; Milani, A.; Magnaghi, P.; Ballinari, D.; Casero, D.; Gasparri, F.; Banfi, P.; Avanzi, N.; Saccardo, M. B.; Alzani, R.; Bandiera, T.; Felder, E.; Donati, D.; Pesenti, E.; Sartore-Bianchi, A.; Gambacorta, M.; Pierotti, M. A.; Siena, S.; Veronese, S.; Galvani, A.; Isacchi, A. The TPM3-NTRK1 rearrangement is a recurring event in colorectal carcinoma and is associated with tumor sensitivity to TRKA kinase inhibition. *Mol. Oncol.* **2014**, *8*, 1495−1507.

(9) Ardini, E.; Menichincheri, M.; Banfi, P.; Bosotti, R.; De Ponti, C.; Pulci, R.; Ballinari, D.; Ciomei, M.; Texido, G.; Degrassi, A.; Avanzi, N.; Amboldi, N.; Saccardo, M. B.; Casero, D.; Orsini, P.; Bandiera, T.; Mologni, L.; Anderson, D.; Wei, G.; Harris, J.; Vernier, J.-M.; Li, G.; Felder, E.; Donati, D.; Isacchi, A.; Pesenti, E.; Magnaghi, P.; Galvani, A. Entrectinib, a Pan-TRK, ROS1, and ALK Inhibitor with Activity in Multiple Molecularly Defined Cancer Indications. *Mol. Cancer Ther.* **2016**, *15*, 628−639.

(10) Berger, S.; Martens, U. M.; Bochum, S. Bochum, S. Larotrectinib (LOXO-101). *Recent Results Cancer Res.* **2018**, *211*, 141−151.

(11) Drilon, A.; Nagasubramanian, R.; Blake, J. F.; Ku, N.; Tuch, B. B.; Ebata, K.; Smith, S.; Lauriault, V.; Kolakowski, G. R.; Brandhuber, B. J.; Larsen, P. D.; Bouhana, K. S.; Winski, S. L.; Hamor, R.; Wu, W.-I.; Parker, A.; Morales, T. H.; Sullivan, F. X.; DeWolf, W. E.; Wollenberg, L. A.; Gordon, P. R.; Douglas-Lindsay, D. N.; Scaltriti, M.; Benayed, R.; Raj, S.; Hanusch, B.; Schram, A. M.; Jonsson, P.; Berger, M. F.; Hechtman, J. F.; Taylor, B. S.; Andrews, S.; Rothenberg, S. M.; Hyman, D. M. A Next-Generation TRK Kinase Inhibitor Overcomes Acquired Resistance to Prior TRK Kinase Inhibition in Patients with TRK Fusion-Positive Solid Tumors. *Cancer Discovery* **2017**, *7*, 963−972.

(12) Drilon, A.; Ou, S.-H. I.; Cho, B. C.; Kim, D.-W.; Lee, J.; Lin, J. J.; Zhu, V. W.; Ahn, M.-J.; Camidge, D. R.; Nguyen, J.; Zhai, D.; Deng, W.; Huang, Z.; Rogers, E.; Liu, J.; Whitten, J.; Lim, J. K.; Stopatschinskaja, S.; Hyman, D. M.; Doebele, R. C.; Cui, J. J.; Shaw, A. T. Repotrectinib (TPX-0005) Is a Next-Generation ROS1/TRK/ALK Inhibitor That Potently Inhibits ROS1/TRK/ALK Solvent-Front Mutations. *Cancer Discovery* **2018**, *8*, 1227−1236.

(13) Diaz, L. A.; Platz, E. A.; Teicher, B. Combating Acquired TRK Inhibitor Resistance. *Cancer Discovery* **2019**, *9*, 684-685. DOI: 10.1158/2159-8290.CD-NB2019-047

(14) Wilson, F. H.; Herbst, R. S. Larotrectinib in NTRK-Rearranged Solid TumorsPublished as part of the Biochemistry series "Biochemistry to Bedside. *Biochemistry* **2019**, *58*, 1555−1557.

(15) Choi, H.-S.; Rucker, P. V.; Wang, Z.; Fan, Y.; Albaugh, P.; Chopiuk, G.; Gessier, F.; Sun, F.; Adrian, F.; Liu, G.; Hood, T.; Li, N.; Jia, Y.; Che, J.; McCormack, S.; Li, A.; Li, J.; Steffy, A.; Culazzo, A.; Tompkins, C.; Phung, V.; Kreusch, A.; Lu, M.; Hu, B.; Chaudhary, A.; Prashad, M.; Tuntland, T.; Liu, B.; Harris, J.; Seidel, H. M.; Loren, J.; Molteni, V. (R)-2-Phenylpyrrolidine Substituted Imidazopyridazines: A New Class of Potent and Selective Pan-TRK Inhibitors. *ACS Med. Chem. Lett.* **2015**, *6*, 562−567.

(16) Duan, S.; Dong, L.; Wang, B.; Wei, S.; Gong, X.; Yu, P.; Li, C.; Gao, Y.; Ye, L.; Wang, H.; Tian, J. Assessment of the toxicity and toxicokinetics of the novel potent tropomyosin receptor kinase (Trk) inhibitor LPM4870108 in rhesus monkeys. *Regul. Toxicol. Pharmacol.* **2021**, *122*, 104886.
(17) Li, F.; Liu, Z.; Sun, H.; Li, C.; Wang, W.; Ye, L.; Yan, C.; Tian, J.; Wang, H. PCC0208017 a novel small-molecule inhibitor of MARK3/MARK4, suppresses glioma progression in vitro and in vivo. *Acta Pharm. Sin. B* **2020**, *10*, 289−300.

https://doi.org/10.1021/acs.jmedchem.1c00712
J. Med. Chem. 2021, 64, 10286−10296